Numerical simulation of the unstable flow phenomenon in a pump turbine at the load rejection conditions in turbine mode

L K Wang[1], W L Liao[1], J L Lu[1], Y P Zhao[1] and H Ruan[1]

[1]Institute of water Resource and hydro-electric Engineering, Xi'an University of Technology, Xi'an, China

E-mail: liaoweili2004@163.com

Abstract. The governor mechanism fails to work when the pump turbine losses the loads suddenly, and the rotating speed of the runner has a quickly increasing. Additionally the unit will jump to the rotating stall condition. In order to study the internal flow field and pressure fluctuation of the pump turbine with different guide vane opening under the rotating stall conditions, a model type pump-turbine of a pumped-storage power station was set as the research object in this paper. And both of the steady and unsteady numerical simulations were carried out to simulate the flow field of the pump-turbine. The internal flow and pressure fluctuation characteristics in guide vane and runner were analysed under the different guide vane opening. The results show that there is an obvious impact at the leading edge of the runner which resulting in the appearance of vortex under the small guide vane opening. With the increasing of the opening and discharge rate, the circumferential crossflow has developed and extended to the vaneless space which blocked the inlet of the runner and disordered the internal flow of the runner. The vortex structures composed of streamwise vortices, horseshoe vortices. The dominant frequency of vaneless space monitor points are 9fn which influenced by RSI under the small guide vane opening and optimal guide vane opening, and 4.75fn which influenced by vortex at great guide vane opening. The pressure fluctuation on pressure and suction surface are affected greatly by the flow pattern inside the runner, there are a lot of low frequency pressure pulsation. The amplitude of all monitor points increased with the increasing of the flow rate.

1. Introduction

With the fast development of new energy such as solar power and wind power, the proportion of new energy in the power grid is increasing. It will adversely affect the safety and stability of the power grid, because of the obvious instability and intermittent which influenced by the environment [1]. The pumped storage power plant has flexible operation ability, fast starting, real-time tracking of load change, and it is an indispensable tool to ensure the safety and stable operation, to respond rapid changes and to realize optimal dispatching of power grid. So this kind of plant can deal with the load change of the electric power system effectively which is very important for the adjustment of the electric grid. As the key equipment of pumped storage power plant, the pump turbine is studied by lots of researchers. Runaway process is an unstable process. When the pump turbine losses the loads suddenly and at the same time, the governor mechanism fails to work which make the guide vanes can't close promptly, and the rotating speed of the pump turbine runner will increase quickly and the maximum speed is decided by the guide vane opening and the water head [2]. The dynamic loads generated by the mass unbalance of the runner and hydraulic unstable phenomenon in flow passage

components increase largely, and that makes the unit in a dangerous condition. It will cause the unit vibration and adversely threat the safety and stable operation of the unit.

Less information is available on rotating stall in turbine operation of pump-turbines. D Anciger [3] discovered three distinct rotating stall cells in the vaneless space in pump mode, and this phenomenon is obviously with the decreasing of the flow rate. Vlad Hasmatuchi [4] investigated the pressure fluctuation at off-design conditions by experiment, and asserted that there is low frequency component and flow separation in the runner channels leading to their blockage at runaway condition. L S Xia [5] argued that rotating stalls lead to the flow in the vane diffuser channels alternating between outward jet flow and blockage. Strong jets impacted the spiral case wall and caused high pressure pulsations. Severe separations of the stall cells disturbed the flow inducing periodical large amplitude pressure fluctuations. Zeng et al. [6] theoretically explored the root cause of the pump-turbine instability under no-load conditions and the dominant factors which influenced it. Furthermore, they provided a mathematical expression for the no-load oscillation and analysed the oscillation characteristics. Vesely´[7] and Staubli [8] both measured one cell rotating stall at large GVOs with a relative frequency of 60% of the rotational frequency.

But analysis on the pump turbine unsteady internal flow characteristic at runaway points with different guide vane openings is uncommonly. Thus, this paper took weakly compressible of water into consideration and focused on the internal flow field and pressure fluctuation analysis at runaway points with different guide vane openings.

2. Pump Turbine Specification

As shown in Figure 1, the whole pump turbine configuration including spiral case, stay vane, guide vane, runner and draft tube is considered in the physical model. The computing domain enables to overcome the influence of boundary conditions, periodic interfaces, and pitch ratio of rotor-stator interface. Specifications of the pump turbine are listed in table.1.

Figure 1. Three-dimensional model of the pump turbine

Table 1. Main specifications of pump turbine

Parameters	value
Runner blade number ZB	9
Guide vane number ZG	20
Stay vane number ZS	20
Experimental rotational speed (rpm)	750
Runner diameter at inlet D1(mm)	468
Runner diameter at outlet D2(mm)	300
Experimental head H(m)	20

3. Mathematical Model and Computational Details

3.1. Turbulence model

In this paper, the SST turbulence model was used to close the Reynolds averaged Navier–Stokes (RANS) solver for the solution of the turbulence flows. The continuity equation and momentum equation are adopted in simulation.

Continuity equation

$$\frac{\partial(\rho u_i)}{\partial x_i} = 0 \tag{1}$$

Momentum equation

$$\rho \frac{\mathrm{D}u_i}{\mathrm{D}t} = \rho F_i - \frac{\partial p}{\partial x_i} + \frac{\partial}{\partial x_j}\left[\mu\left(\frac{\partial u_i}{\partial x_j} + \frac{\partial u_j}{\partial x_i}\right)\right] + \frac{\partial}{\partial x_i}\left(\lambda \nabla \cdot v\right) \tag{2}$$

3.2. Compressible model

In engineering application, given the constant temperature and the compressibility of water is always represented by the bulk modulus of elasticity, which is defined as:

$$K = dp / \left(d\rho / \rho\right) \tag{3}$$

$$K = \left(p - p_0\right) / \left(\left(\rho - \rho_0\right) / \rho\right) \tag{4}$$

$$\rho = \rho_0 / \left(1 - \frac{p - p_0}{K}\right) \tag{5}$$

Where p is the static pressure and ρ is the density of water and K is the modulus of elasticity.

Under the operating conditions for hydraulic machinery, the modulus of elasticity can be assumed to be constant. In the present study, K=2×10^{9}Pa, p_0=101325Pa and ρ_0=998kg/m^3. By means of user defined function, the variable sound speed is linked to the flow solver CFX.

3.3. Grid generation

Mesh generation is an important step in the numerical discretization of flow control equations, so the mesh quality has a crucial impact on the accuracy of the calculation results. Computational fluid dynamics (CFD) calculations at the design point were repeated on five grids with increasing size. The corresponding efficiency calculated with five grids, were plotted in figure 2.

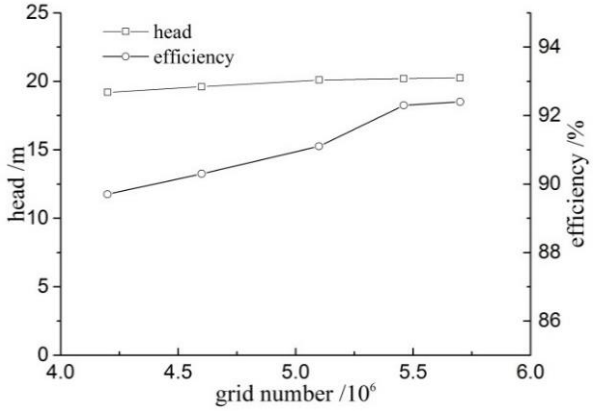

Figure 2. Mesh independence

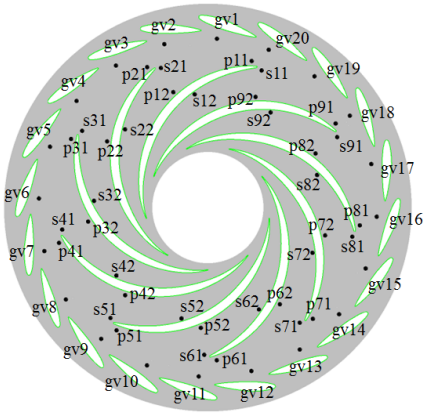

Figure 3. Locations of monitoring points

In this paper, the structured grid is adopted, and mesh independence is carried out. The total number of grid elements is about 5.46 million, the mesh number of each part as shown in table 2.

Table 2. The grid number of the computational domain

	Spiral case	Stay vane	Guide vane	Runner	Draft tube	total
Mesh number(*10^6)	0.26	1.05	1.45	1.80	0.8	5.46

3.4. Boundary condition and monitor points

- Inlet condition. The mass flow inlet at the spiral case of pump turbine is used.
- Outlet condition. Pressure outlet is used at the draft tube of pump turbine, static pressure is specified for all cases.
- Other boundary conditions. No-slip condition has applied on the all solid walls, and standard wall function is used to calculate the turbulence kinetic energy and turbulence dissipation frequency near the wall.
- Time step. During the numerical simulations, the results of steady RANS simulations were used as the initial flow field for the transient simulations. Vlad Hasmatuchi [9] compared unsteady numerical results of the three time steps that runner rotated 2, 1, 0.5 degree spent and argued that the time step which runner rotates 1 degree is reasonable in terms of computation time and accuracy. So the time that runner rotated 1 degree spent is adopted as the time step.

3.5. Calculation conditions

The numerical simulation of inflow pattern in pump turbine at different load rejection conditions are calculated in this paper in table 3. For convinence the operating conditions are plotted using unit parameters, which for hydro-turbines are defined as follows. The unit speed and unit flow rate is

$$n11 = nD/\sqrt{H} \tag{6}$$

$$Q11 = Q/D^2\sqrt{H} \tag{7}$$

Where D is runner diameter at outlet, H is the net head across the pump turbine, n is the speed of runner in rpm/min and Q is the volume flow rate in m^3/s.

In order to obtain the pressure pulsation characteristics of pump turbine at load rejection conditions, there are 20 monitoring points arranged between the guide vane and runner and 36 monitoring points in the blade pressure and suction surface. The details of monitoring points are as shown in Figure 3.

Table 3. Calculation condition points

Calculation points	GVO θ (º)	n11 (rpm/s)	Q11 (m^3/s)
OP1	10	70.398	0.387
OP2	18	66.279	0.275
OP3	26	58.835	0.160

4. Calculation results and Discussion

4.1. Internal flow

Figure 4 shows an overview of the flow field complexity inside the instantaneous distributor and impeller channels by streamlines plotted from numerical results and figure 5 shows the relative flow angle at OP1 OP2 and OP3 respectively. For OP1 the runner inlet flow angle was smaller than the blade angle and the incidence angle is negative, which caused the greater impact on the blade inlet edge. It can be observed that vortex exists on every blade inlet pressure surface in the numerical simulations and flow separation exists on suction surface. For OP2 the runner inlet flow angle was close to the blade angle with the increase of guide vane opening. The rotating flow separations develop initially in the impeller channels. The circumferential crossflow develop and extend to the vaneless space between impeller and guide vanes which blocked the inlet of runner and disordered the internal

flow of runner. And obvious flow separation and reflux on the suction surface of blade can be observed. For OP3 the runner inlet flow angle is obviously greater than blade angle, the vortex in the vaneless space extended to the guide vane region and had a greater influence on the flow field. It can also be observed that obvious vortex exists on blade inlet and a complete vortex structure is formed on the suction surface.

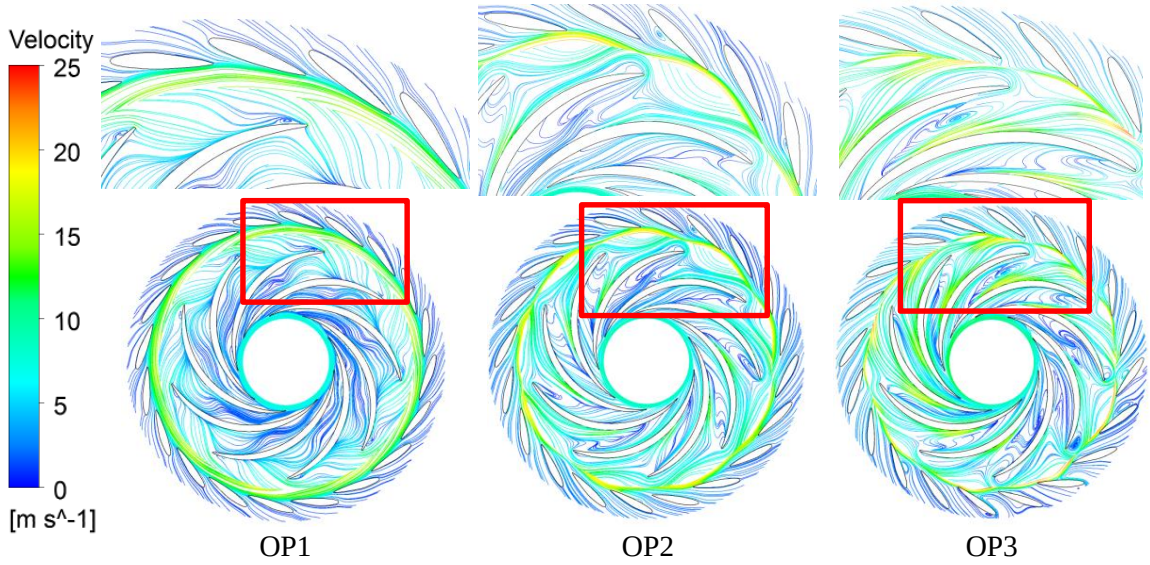

Figure 4. Streamline distribution on the midsection of runner, Span = 0.50

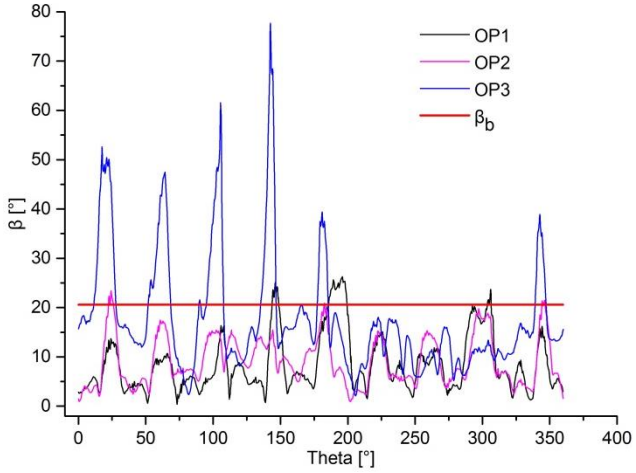

Figure 5. The relative flow angle β in different conditions

For the present study, the structure of the vortex features a strong asymmetry, making the use of simple analytical vortex models impossible for the identification of the vortex characteristics, such as the vortex core radius and the vortex circulation. However, the large-scale vortical structures can be identified by different techniques. For instance, the vorticity is a good and common indicator for the presence of vortices. However, in complex flows, a region of high vorticity does not necessary feature a swirling motion, as a region of strong shear can also exhibit a high vorticity. Alternatively, *Q*-criterion [10] is used to identify the vortex stucture, which is defined as:

$$Q = \frac{1}{2}\left(\Omega_{ij}\Omega_{ij} - S_{ij}S_{ij}\right) \tag{8}$$

Where Ω is the rate-of-rotation tensor and S is the rate-of-strain tensor.

An instantaneous iso-surface of the *Q*-criterion in the guide vane and runner is shown in Figure6. The usage of this identification can visualize the inception and evolution of the rotating stall in 3-D space. The vortex structures compose streamwise vortices, horseshoe vortices. And the vortex structure in the vaneless space is greater complex with the increase of the opening. For OP1 it can be observed vortex in the vaneless space, but there is almost no vortex inside the runner. For OP2 the streamwise vortices appear in almost every flow passage besides the vortex structure in the vaneless space. For OP3 both the vortex structure region and the intensity increase because of the greater discharge. It can also be observed that obvious complete vortex structure is formed on the suction surface that is consistent with the analysis of the streamlines.

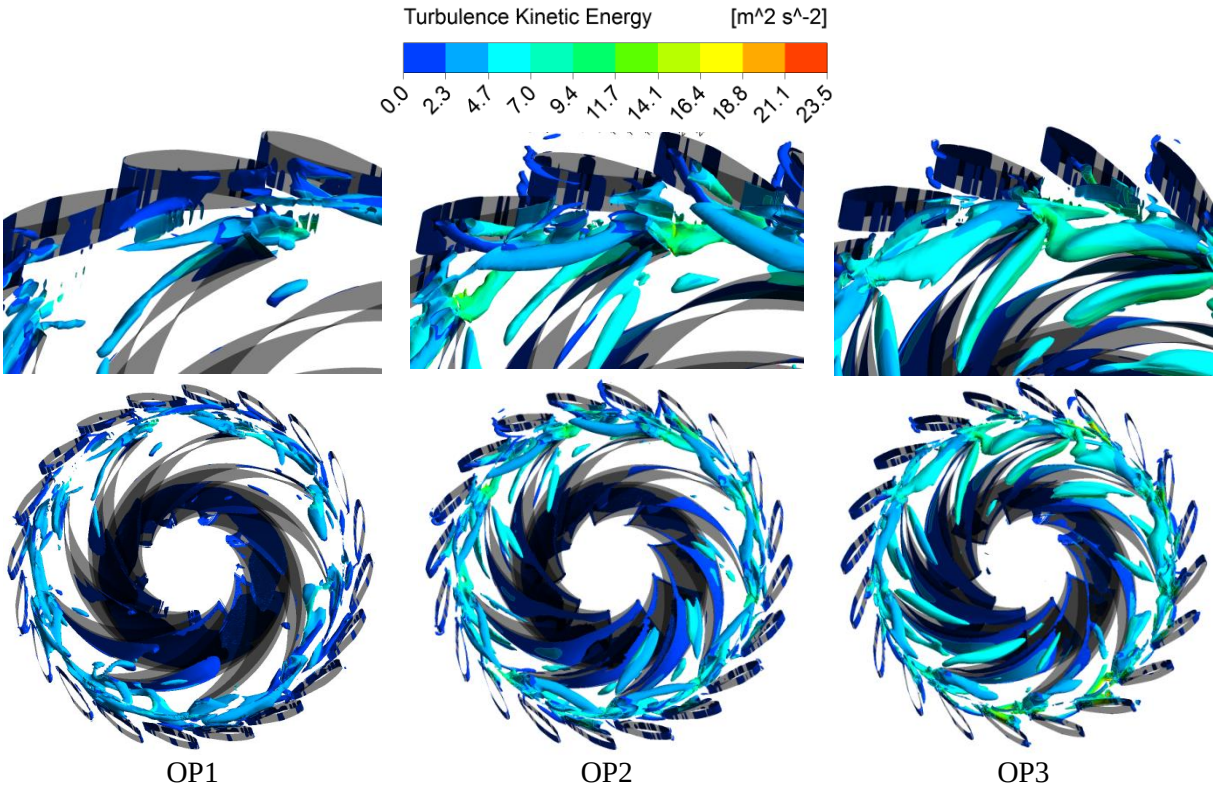

Figure 6. Flow vortex structures within vane diffuser channels (Q=560000s^{-2})

Form the above analyse, it can be found that the flow pattern in each flow passage of the runner is unevenly distributed. In order to describe the heterogeneity, the discharges of every flow passage in one revolution are plotted in figure 7 and the yellow line represents the average of the calculated discharge. The discharge in every flow passage is quite different at the same time. Such as the discharge of P2 is almost 2.5 times as much as the P7. For OP1 the discharge of each flow passage is almost periodically distributed in one revolution, and the number of cycles is equal to the number of blades. But there is almost no periodicity for OP2 and OP3 which is due to a large number of unsteady vortex structures in the runner.

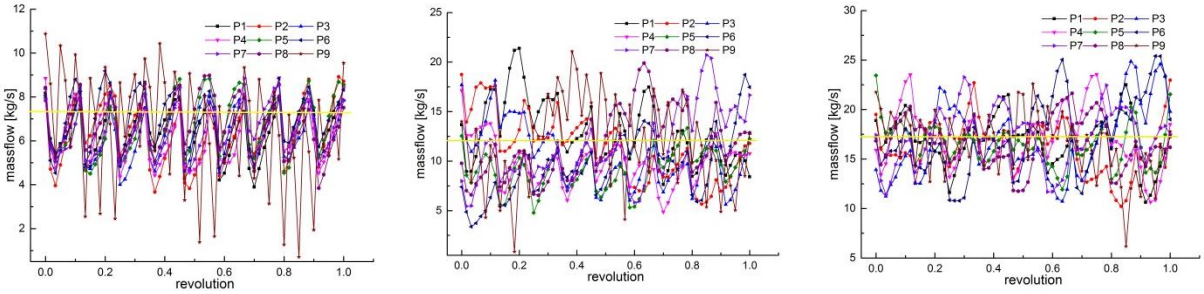

OP1 OP2 OP3

Figure 7. Discharge distribution in each passage under different conditions

4.2. Pressure fluctuation

This paper introduced the dimensionless number C_p (pressure fluctuation coefficient) in the treatment of pressure fluctuation data of various monitoring points, the definition of C_p as shown in equation (9), it represents the percentage of pressure fluctuation in head size.

$$C_p = \frac{\Delta P}{\rho g H} \times 100\% \tag{9}$$

Where $\Delta P = P - \bar{P}$ is the amplitude of pressure fluctuation, P is the pressure of numerical simulation, $\bar{P}$ is the average pressure of numerical simulation, ρ is the density of water, H is the head of operating condition.

In order to study the pressure pulsation of monitoring points at different guide vane opening, the analysis of amplitude and frequency of the pressure pulsation is carried out. The spectral characteristics of different monitoring points at different conditions are analysed. The rotating frequency of runner fn are 14.62Hz, 16.47Hz and 17.49Hz respectively, and the blade passing frequency 9fn is equal to the product of rotating frequency and blade number.

4.2.1. Pressure fluctuation in vaneless space. Figure 8 shows the time domain of pressure fluctuation in vaneless space, and it can be observed that the pressure fluctuation shows obvious periodicity. The range of pressure fluctuations gradually increased with the increase of guide vane opening and discharge. The frequency map of each monitor point is obtained as shown in figure 9 by FFT.

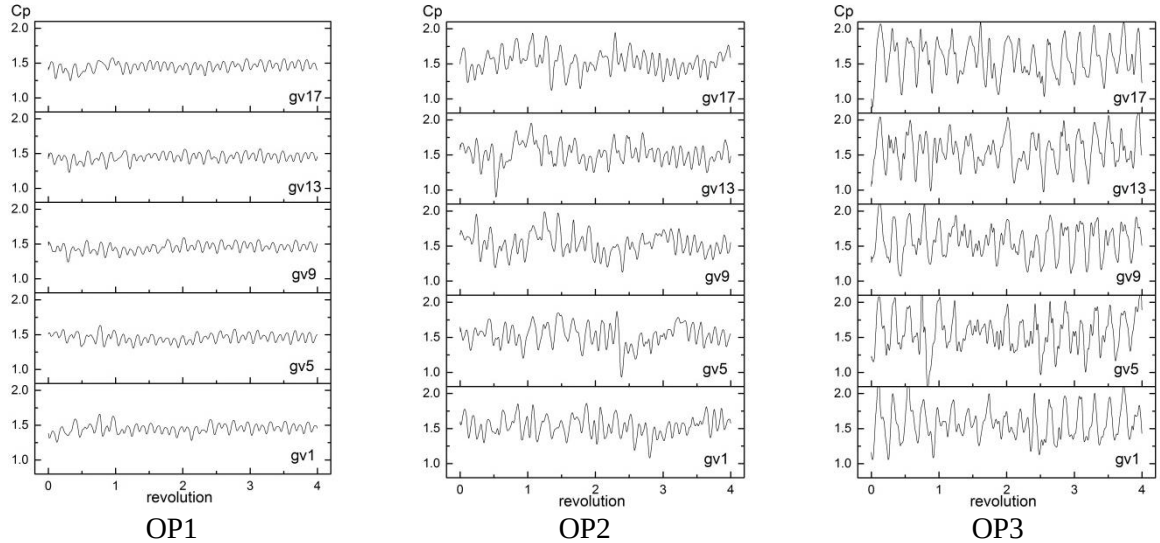

OP1 OP2 OP3

Figure 8. Pressure fluctuation time domain in vaneless space

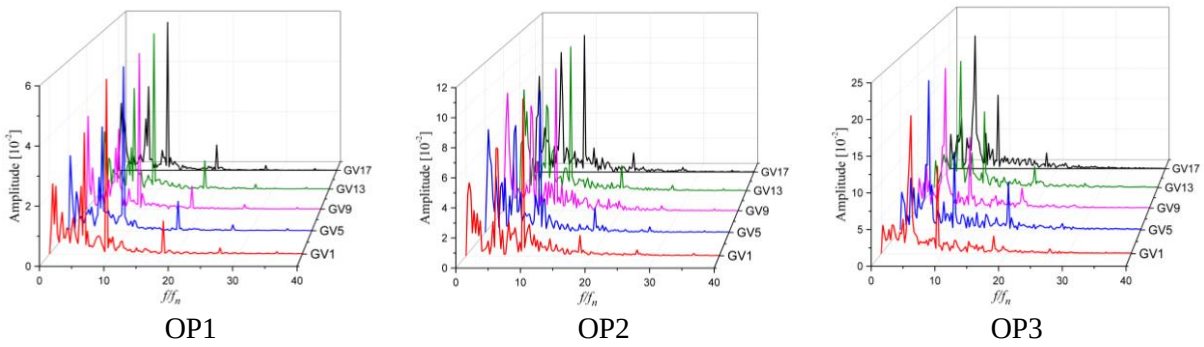

Figure 9. Pressure pulsation frequency domain in vaneless space

The dominant frequency is blade passing frequency because of the RSI between the guide vane and runner at OP1 and OP2, but the 4.75fn for OP3 because of the great influence of circumferential crossflow. The second frequency is 9fn. The amplitude of each guide vane monitor points (gv1~gv20) is basically equal at OP1 because the flow pattern in guide vane zone is smooth and no vortex appear, but the amplitude is serrate for OP2 and OP3 whether the main frequency or sub frequency, which is caused by uneven flow in the circumferential direction. And there are a lot of low frequency and high frequency pressure pulsation at all calculation conditions, such as 0.5fn, 0.75fn, 18fn and 27fn. The pressure fluctuation amplitude of all measuring points increases with the increase of the opening, which is due to the increase of the flow rate and the deterioration of the flow regime.

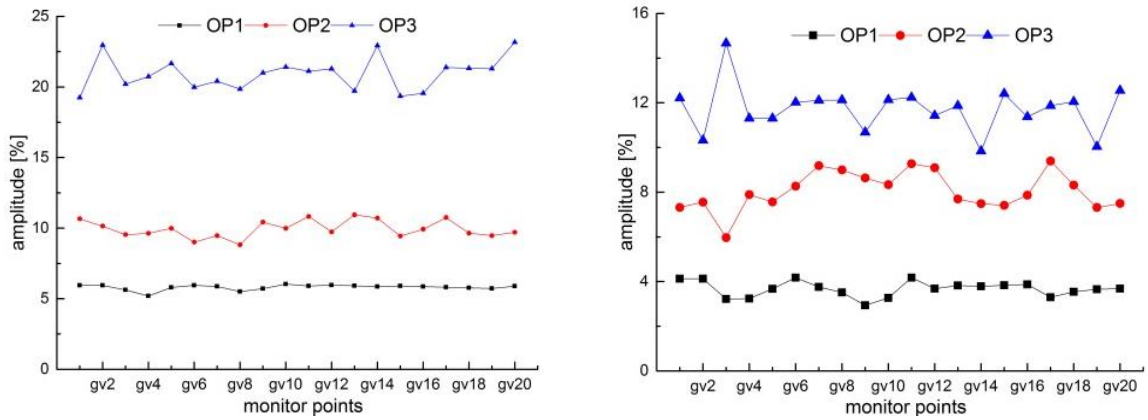

Figure 10 Amplitude of dominant frequency (lift) and second frequency (right)

4.2.2. Pressure fluctuation in blade. On the blade pressure surface, the pressure pulsation characteristics of the monitoring points are plotted in figure 11. For OP1 the dominant frequencies of pressure fluctuations include 0.5fn and 5.5fn, which is duo to the great impact of the runner inlet and the formation of vortex at the blade inlet. For OP2 the flow field is defferent on every blade pressure surface. Such as there is almost no streamwise vortricity in P7/P8/P9, while other passages exist obviously. So the dominant frequencies of pressure fluctuation include 0.5fn, 4.75fn and 5fn. For OP3 although there is a large number of vortex sturctures in the rnner, but the dominant frequency of all monitor points are 4.75fn.

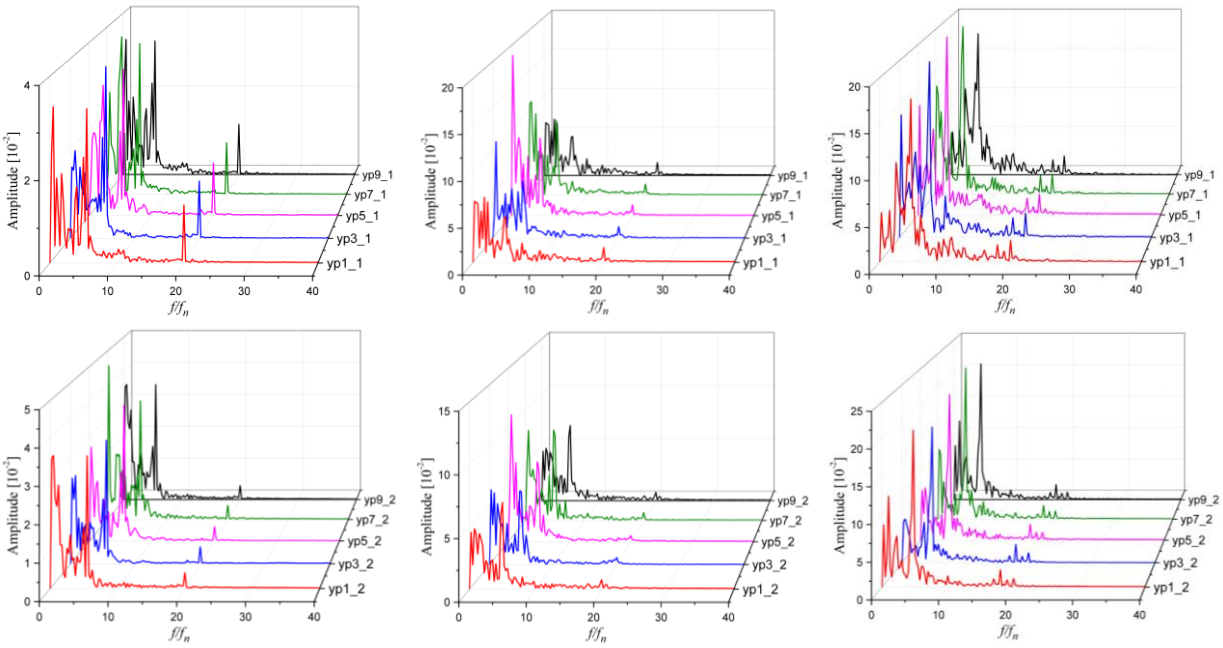

Figure 11. Pressure pulsation frequency domain on pressure surface of blade

On the blade pressure surface, the pressure pulsation characteristics of the monitoring points are plotted in figure 12. There is almost no vortex on the suction surface at OP1, so the dominant is 5.5fn. But the dominant frequenceies are relative complex at OP2, and these include 0.5fn, 1.25fn, 4.75fn and 5fn. The dominant frequencies on suction surface are 4.75fn which are the same as pressure surface.

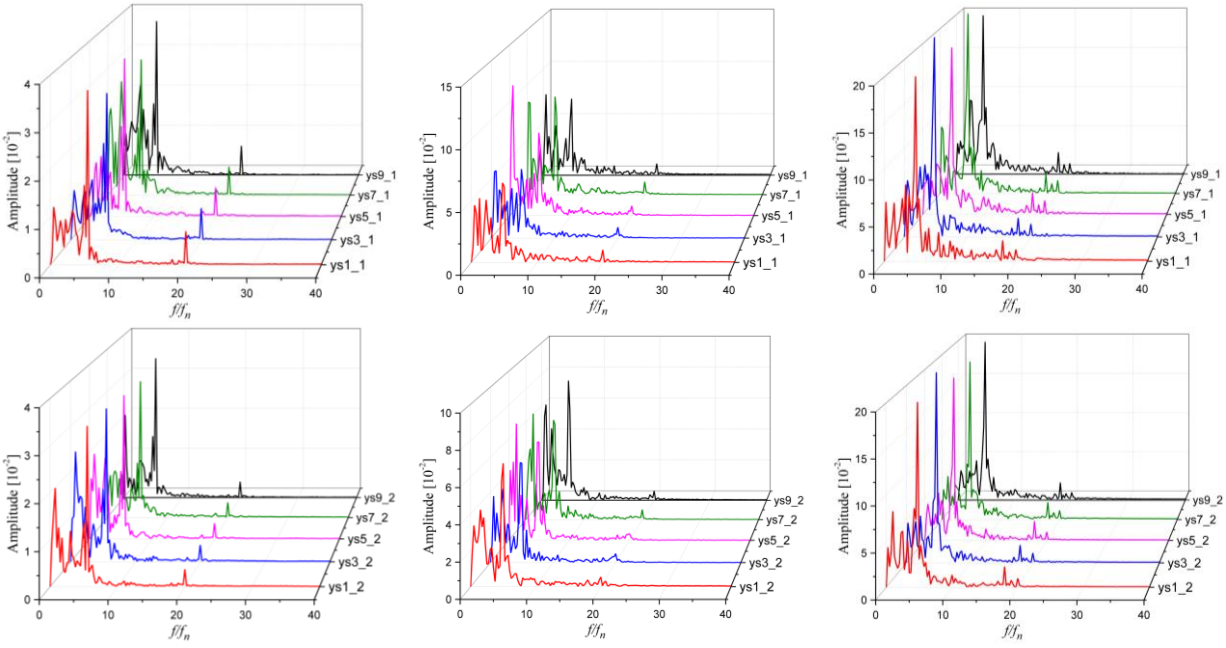

Figure 12. Pressure pulsation frequency domain on pressure surface of blade

5. Conclusion

The comprehensive calculation of pump turbine at load rejection conditions are carried out in this paper by using the numerical simulation method. And the analysis of flow field and pressure pulsation were also carried out. Comparison and analysis of calculation results of different calculation conditions were conducted, and the following conclusions can be drawn:

The negative incidence angle caused the greater impact on the leading edge of the blade and vortex exists on every blade inlet pressure surface at OP1. For OP2 the circumferential crossflow developed and extended to the vaneless space between impeller and guide vanes which blocked the inlet of runner and disordered the internal flow of runner. For OP3 the vortex in the vaneless space extended to the guide vane region and had a greater influence on the flow field. The vortex structures composed of streamwise vortices, horseshoe vortices.

The dominant frequency is blade passing frequency because of the RSI between the guide vane and runner at OP1 and OP2, but the 4.75fn for OP3 because of the great influence of circumferential crossflow. The second frequency is 9fn. The amplitude of each guide vane monitor points (gv1~gv20) is basically equal at OP1, but the amplitude is serrate for OP2 and OP3 whether the main frequency or sub frequency. And there are a lot of low frequency and high frequency pressure pulsation at all calculation conditions, such as 0.5fn, 0.75fn, 18fn and 27fn.

For OP1 the dominant frequencies of pressure fluctuations include 0.5fn and 5.5fn, which is due to the great impact of the runner inlet and the formation of vortex at the blade inlet. For OP2 the flow field is different on every blade pressure surface. So the dominant frequencies of pressure fluctuation include 0.5fn, 4.75fn and 5fn. For OP3 although there is a large number of vortex structures in the runner, but the dominant frequency of all monitor points are 4.75fn.

Acknowledgments

So long and thanks for all the supports from the National Natural Science Foundation of China (51679196, 51339005, 51379174, 51279260).

References

[1] S. E. He and Xi. Z Dong. 2012 Cause analysis on large-scale wind turbine tripping and its countermeasures 131-137.
[2] Li J W, L S H, Wu Y L, et al. 2009 *J. of Hydroelectric Engineering* 28 178-182
[3] D Anciger, A jung and T Aschenbrenner. 2010 Prediction of rotating stall and cavitation inception in pump turbines 25th IAHR Symposium on Hydraulic Machinery and Systems (Timisoara Romania)
[4] Vlad Hasmatuchi. 2009 Experimental investigation of a pump turbine at off design operation conditions 3rd IAHR International Meeting of the Workgroup on Cavitation Symposium on Hydraulic Machinery and Systems.
[5] L S Xia, Y G Cheng, X X Zhang et al. 2014 Numerical analysis of rotating stall instabilities of a pump turbine in pump mode 27th IAHA symposium on Hydraulic Machinery and Systems.
[6] Zeng Y H, Yang J Z Guo W C 2015 Runaway instability of pump turbines in S-shaped regions considering water compressibility *J Fluids Eng – Trans* ASME 0501401
[7] Vesely J, Pulpitel L and Troubil P 2006 Model research of rotating stall on pump turbines Hydro Power and Dams.
[8] Staubli T 1987 Some results of force measurements on the impeller of a model pump turbine IAHA symposium on Hydraulic Machinery and Systems.
[9] Vlad Hasmatuchi. 2012 Hydrodynamics of a pump-turbine operating at off-design conditions in generating mode. EPFL
[10] Jeong J and hussain F 1995 On the identification of a vortex J. fluid mechanics 285 69-94
[11] L K Wang, W L Liao and J L Lu 2017 Pressure fluctuations in pump turbines in S zone based on weakly compressible modelling *J of Hydroelectric Engineering.* 36(6) 69-78